# AMSR-E Algorithm Theoretical Basis Document: Sea Ice Products

Thorsten Markus and Donald J. Cavalieri
Hydrospheric and Biospheric Sciences Laboratory
NASA Goddard Space Flight Center
Greenbelt, MD 20771

## 1. Overview

The AMSR-E sea ice standard level 3 products include sea ice concentration, sea ice temperature, and snow depth on sea ice. The AMSR-E standard sea ice concentration product is generated using the enhanced NASA Team (NT2) algorithm described by Markus and Cavalieri (2000), the snow depth is produced from the algorithm described by Markus and Cavalieri (1998) for both hemispheres, but excluding the Arctic perennial ice regions, and the ice temperature is produced from an algorithm similar to the Nimbus 7 Scanning Multichannel Microwave Radiometer (SMMR) sea ice temperature algorithm described by Gloersen et al. (1992). Additionally, the difference between the Bootstrap algorithms (see ATBD by J.C. Comiso) and the NT2 retrieved concentrations (Bootstrap-NT2) are archived. These products together with AMSR-E calibrated brightness temperatures (TBs) are mapped to the same polar stereographic projection used for SSM/I data to provide the research community consistency and continuity with the existing 28-year Nimbus 7 SMMR and DMSP SSM/I sea ice concentration products. The grid resolutions are as follows: (a) TBs for all AMSR-E channels: 25-km, (b) TBs for the 18, 23, 36, and 89 GHz channels: 12.5-km, (c) TBs for the 89 GHz channels: 6.25-km, (d) Sea ice concentration: 12.5-km, 25-km, (e) Sea ice temperature: 25-km, (f) Snow depth on sea ice: 12.5 km. All of these products are stored as a composite of (i) daily-averaged ascending orbits only, (ii) daily-averaged descending orbits only, and (iii) all orbits creating a full daily average.

## 2. Sea ice concentration

### 2.1. Algorithm

The two ratios of brightness temperatures used in the standard NT algorithm (Cavalieri et al., 1984) as well as in the NT2 approach are the polarization

$$PR(\nu) = [TB(\nu V) - TB(\nu )] / [TB(\nu V) + TB(\nu H)]$$

and the spectral gradient ratio

$$GR(\nu 1p\nu 2p) = TB(\nu 1p) - TB(\nu 2p)] / [TB(\nu 1p) + TB(\nu 2p)]$$

where TB is the brightness temperature at frequency ν for the polarized component p (vertical (V) or horizontal (H)). Figure 1a shows a typical scatterplot of PR(19) versus GR(37V19V) for September conditions in the Weddell Sea. The NT algorithm identifies two ice types, which are associated with first-year and multiyear ice in the Arctic and ice types A and B in the Antarctic (as shown in Figure 1a). The A-B line represents 100% ice concentration. The distance from the open water point (OW) to line A-B is a measure of the ice concentration. In this algorithm, the primary source of error is attributed to conditions in the surface layer such as surface glaze and layering (Comiso et al., 1997), which can significantly affect the horizontally polarized 19 GHz brightness temperature (Matzler et al., 1984) leading to increased PR(19) values and thus underestimates in ice concentration. In the following, we will call these surface effects. In Figure 1a, pixels with significant surface effects create a cloud of points underestimating ice concentrations (labeled C). The use of the SSM/I horizontally polarized channels makes it imperative to resolve a third ice type to overcome the difficulty of surface effects on the emissivity of the horizontally polarized component.

Our approach makes use of the 89 GHz channels, because the horizontally polarized 89 GHz data are much less affected by surface effects than the horizontally polarized 19 GHz data (Matzler et al., 1984) and the 89 GHz channels have successfully been used in sea ice concentration retrievals under clear atmospheric conditions [Lubin et al., 1998]. Here we use the 89 GHz channels together with a forward radiative transfer model to provide ice concentrations under all atmospheric conditions. We make use of GR(89V19V) and GR(89H19H) to resolve the ambiguity between pixels with true low ice concentration and pixels with significant surface effects. A plot of these two ratios are found to form two narrow clusters of points (labeled A-B and open water) as well as a more diffuse cluster of points (labeled C) where surface effects decrease TB(19H) and consequently increase GR(89H19H) (Figure 1b). Values of high GR(89V19V) and high GR(89H19H) are indicative of open water; the range of GR(89H19H) values is larger because of the greater dynamic range between ice and water for the horizontally polarized components. With increasing ice concentration, the two ratios have more similar values. The narrow cluster of pixels adjacent to the diagonal shown in Figure 1b represents 100% ice concentration with different GR values corresponding to different ice types. When surface effects come into play, points deviate from this narrow cluster towards increased GR(89H19H) values (cloud of points to the right of the diagonal) while GR(89V19V) remains constant. This cloud of points labeled C in Figure 1b also corresponds to the cluster of points labeled C in Figure 1a. The difference, therefore, between these two GRs (ΔGR) is a measure of the impact of surface effects on the retrieval. The use of the 89 GHz data requires a correction for atmospheric effects. The use of PR(89) provides this additional information to unambiguously distinguish weather effects from changes in sea ice conditions.

Figure 2a shows the general flow of the algorithm. First brightness temperatures are calculated for the four surface types and all weather conditions (currently 12). The response of the brightness temperatures to different weather conditions is calculated using an atmospheric radiative transfer model (Kummerow, 1992). Input data into the model are the emissivities of the different surface types (taken from Table 4-1 in Eppler

et al. (1992)) with modifications to achieve agreement between modeled and observed ratios), different cloud properties (specifically cloud base, cloud top, cloud liquid water) that are taken from Fraser et al. {1975), and average atmospheric temperature and humidity profiles for summer and winter conditions (taken from Antarctic research stations). We calculate brightness temperatures for all possible ice concentration combinations in 1% increments and for each solution calculate the ratios $PR_R(19)$, $PR_R(89)$ (89 for AMSR-E), and $\Delta GR$. This creates a prism in which each element within this space contains a vector with the three ratios: $PR_R(19)$, $PR_R(89)$, and $\Delta GR$ (Figure 2b). The subscript R refers to a rotation of axes in PR-GR space (Figure 1a) by the angle $\varphi$ so that $PR_R(19)$ and $PR_R(89)$ are independent of ice types A and B in the Antarctic, and first-year and multiyear ice for the Arctic. For each pixel the observed brightness temperatures are used to create a vector with the same ratios. We then move through this prism comparing the observed three ratios with the modeled ones. The indices where the differences are smallest determine the final ice concentration combination and weather index. While for the Antarctic the algorithm resolves fractions between ice types A/B, C, and open water, in the Arctic we also resolve a thin ice type. Using a GR(37V19V) threshold of -0.02 we either resolve ice type C (for pixels where GR(37V19V)) is below this threshold or thin ice (for pixels where GR(37V19V) is above this threshold. A limitation, of course, is that we cannot resolve mixtures of thin ice and thicker ice with layering.

### 2.1. Implementation

NT2 sea ice concentrations are calculated using the individual Level 2A swaths rather than using gridded averaged brightness temperatures in order to make the atmospheric corrections on an orbit-by-orbit basis before obtaining daily average ice concentrations.

A weather filter following Gloersen and Cavalieri (1986) and Cavalieri et al. (1995) is applied in order to eliminate spurious weather effects over the open ocean.

Although a land mask is applied to the ice concentration maps land spillover still leads to erroneous ice concentrations along the coast lines adjacent to open water. This makes operational usage of these maps cumbersome. Therefore, we apply a land spillover correction scheme on the maps. The challenge is to delete all erroneous ice concentrations while at the same time preserving actual ice concentrations, as for example, along the margins of costal polynyas (Figure 3 shows an example).

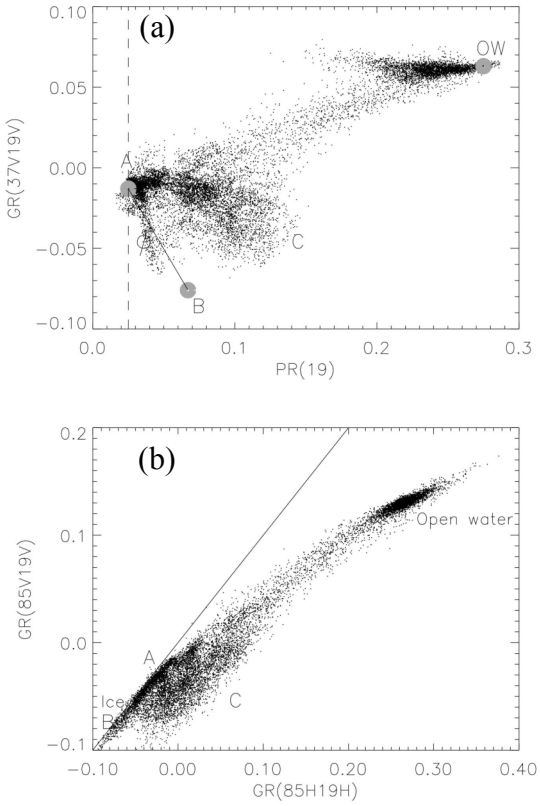


Figure 1: a) GR(37V19V) versus PR(19) for the Weddell Sea on September15, 1992. The gray circles represent the tiepoints for the ice types A and B as well as for open water as used by the NT algorithm. Label C indicates pixels with significant surface effects. $\phi$ is the angle between the y-axis and the A-B line. b) GR(89V19V) versus GR(89H19H). The ice types A and B are close to the diagonal. The amount of layering corresponds to the horizontal deviation from this line towards label C

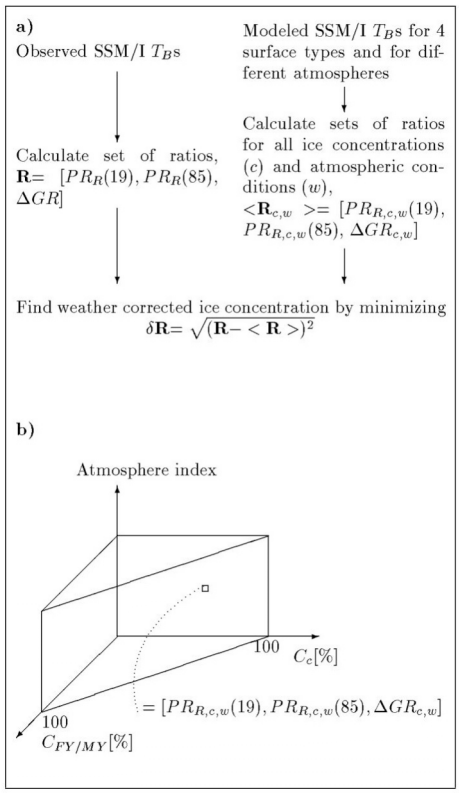


Figure 1: Flow diagram of NT2 algorithm (from Markus and Dokken, 2002).

without land spillover correction

with land spillover correction

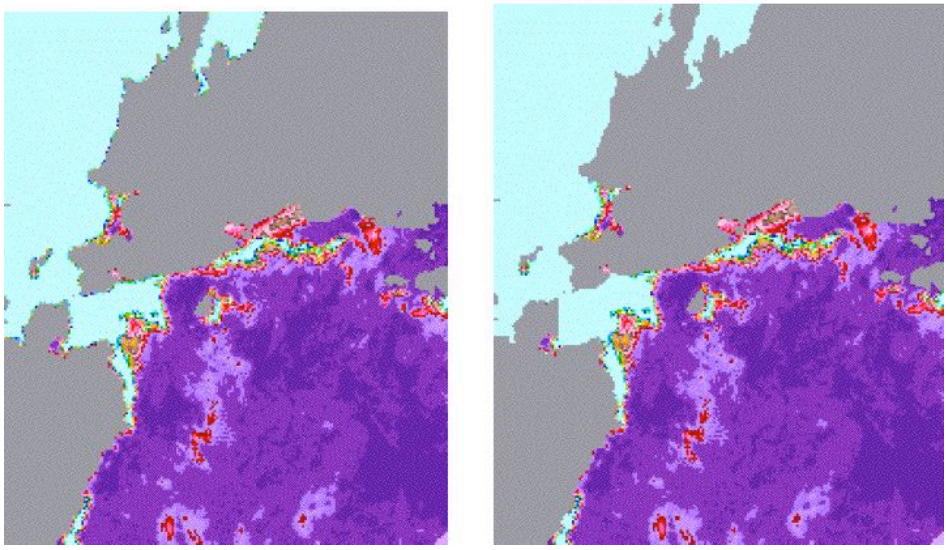

**Figure 2: Map of ice concentration without and with land spillover correction.**

## 3. Snow depth on sea ice

### 3.1. Algorithm

The AMSR-E snow-depth-on-sea-ice algorithm was developed using DMSP SSM/I data (Markus and Cavalieri, 1998) to estimate snow depth on sea ice from space. The snow depth on sea ice is calculated using the spectral gradient ratio of the 18.7 GHz and 37 GHz vertical polarization channels,

$$h_s = a_1 + a_2 \, GRV(ice)$$

where hs is the snow depth in meters, and $a_1$=2.9 and $a_2$=-782 are coefficients derived from the linear regression of *in situ* snow depth measurements on microwave data. GRV(ice) is the spectral gradient ratio corrected for the sea ice concentration, C, as

follows:

$$GRV(ice) = [T_B(37V)-T_B(19V)-k_1(1-C)] \ / \ [T_B(37V)+T_B(19V)-k_2(1-C)]$$

with $k_1=T_{BO}(37V)-T_{BO}(19V)$ and $k_2=T_{BO}(37V)+T_{BO}(19V)$. The open water brightness temperatures, $T_{BO}$, are average values from open ocean areas and are used as constants. The principal idea of the algorithm is similar to the AMSR-E snow-on-land algorithm (Kelly et al., 2003) utilizing the assumptions that scattering increases with increasing snow depth and that the scattering efficiency is greater at 37 GHz than at 19 GHz. For snow-free sea ice, the gradient ratio is close to zero and it becomes more and more negative as the snow depth (and grain size) increases. The correlation of regional *in situ* snow depth distributions and satellite-derived snow depth distributions is 0.81 (Figure 4). The upper limit for snow depth retrievals is 50 cm which is a result of the limited penetration depth a 19 and 37 GHz.

### 3.1. Implementation

The algorithm is applicable to dry snow conditions only. At the onset of melt, the emissivity of both the 19 GHz and the 37 GHz channels approach unity (that of a blackbody) and the gradient ratio approaches zero initially before becoming positive. Thus, snow depth is indeterminate under wet snow conditions. Snow, which is wet during the day, frequently refreezes during the night. This refreezing results in very large grain sizes (Colbeck, 1982) which leads to a reduced emissivity at 37 GHz relative to 19 GHz thereby decreasing GRV(ice) and thus leads to an overestimate of snow depth. These thaw-freeze events, therefore, cause large temporal variations in the snow depth retrievals. This temporal information is used in the algorithm to flag the snow depths as unretrievable from those periods with large fluctuations.

As grain size *in situ* measurements are even less frequently collected than snow depth measurements, the influence of grain size variations could not be incorporated into the algorithm. Because of the uncertainties in grain size and density variations as well as sporadic weather effects, AMSR-E snow depth products will be 5-day averages similar to the snow-on-land product.

Snow depths are retrieved for the entire Southern Ocean, but only for the seasonal sea ice zones in the Arctic, because the microwave signature of snow is very similar to the multiyear ice signature so that snow depth on multiyear ice cannot be retrieved unambiguously. A multiyear ice mask based on a threshold in GR and on using temporal information is used to flag multiyear ice.

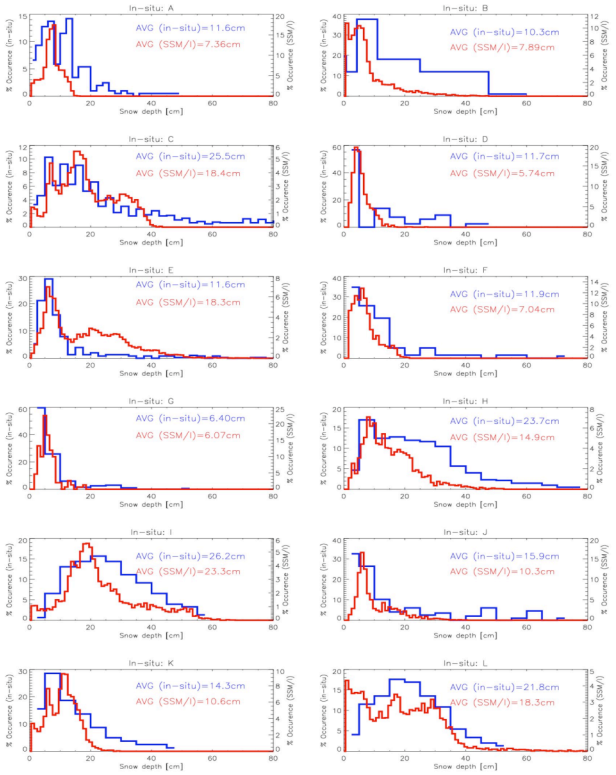


A: **Weddell Sea** **7/86 - 9/86**
*(Wadhams et al., 1986)*
B: **East Antarctic** **10/88 - 12/88**
*(Allison et al., 1993)*
C: **Weddell Sea** **9/89 - 10/89**
*(Eicken et al., 19994)*
D: **East Antartic** **11/91**
*(Worby and Massom, 1991)*
E: **Weddell Sea** **6/92 - 7/92**
*(Drinkwater and Haas, 1994)*
F: **East Antarctic** **10/92 - 11/92**
*(Worby and Massom, 1995)*
G: **East Antarctic** **3/93 - 5/93**
*(Worby and Massom, 1995)*
H: **Bellingshausen** **8/93 - 9/93**
*(Worby et al., 1996)*
I: **Amundsen** **9/94 - 10/94**
*(Sturm et al., 1998)*
J: **East Antarctic** **9/94 - 10/94**
*(Jeffries et al., 1995)*
K: **Ross Sea** **5/95 - 6/95**
*(Sturm et al.,1998)*
L: **Ross Sea/Bellingshausen 8/95-9/95**
*(Sturm et al., 1998)*

**Figure 3: Comparison of *in-situ* and SSM/I-derived snow depth distributions [from Markus and Cavalieri, 1998].**

## 4. Sea Ice temperature

### 4.1. Algorithm

The AMSR-E sea ice temperature is derived from the 6 GHz vertical polarization brightness temperatures following Gloersen et al. (1992) using the simple relationship between ice temperature Ti, the observed brightness temperature at 6 GHz V-pol. TB6V, and the ice emissivity, e:
T_i=TB6V/e.

A constant value of 0.98 is assumed for the ice emissivity. At 6 GHz, there is no emissivity difference between first-year and multiyear ice (see e.g. Gloersen et al., 1992). The retrieved ice temperatures are not surface temperatures but represent a weighted mean temperature of the radiating portion of the ice. For first-year ice, this temperature is close to the snow/ice interface temperature, whereas for multiyear ice, the temperature is a weighted mean of the entire freeboard portion of the ice, with much of the weight at the sea level where a significant fraction of brine remains trapped by the ice (Cavalieri et al., 1984).
A limitation of this algorithm is that it does not take into account variations in emissivity due to surface conditions. Another limitation is that the retrievals are limited to areas of high sea ice concentrations.

### 4.2. Implementation

The ice temperature product is derived for the entire Artic and Antarctic for pixels where the sea ice concentration is greater than 80%. In typical areas of low ice concentration, such as in the marginal sea ice zone and in coastal polynyas, small-scale sea ice and snow cover variability could lead to large errors in the ice temperature product.

## 5. References


Cavalieri, D.J., P. Gloersen, and W.J. Campbell, Determination of sea ice parameters with the NIMBUS 7 scanning multichannel microwave radiometer, J. Geophys. Res., 89, 5355-5369, 1984.

Cavalieri, D. J., K. St. Germain and C. T. Swift, Reduction of Weather Effects in the Calculation of Sea Ice Concentration with the DMSP SSM/I, *J. Glaciology*, 41, 455-464, 1995.

Colbeck, S.C., An overview of seasonal snow metamorphism", *Rev. Geophys. Space Phys.,* Vol. 20, pp. 45-61, 1982.

Comiso, J. C., D. J. Cavalieri, C. L. Parkinson, and P. Gloersen, Passive microwave algorithms for sea ice concentration - A comparison of t wo techniques, Remote Sens. Environ., 60, 357-384, 1997.

Eppler, D.T., and 14 others, Passive microwave signatures of sea ice, in Microwave Remote Sensing of Ice, Geophys. Monogr. Ser., vol. 68, edited by F. Carsey, pp. 47-71, AGU, Washington, D.C., 1992.

Fraser R.S., Gaut, N.E., Reifenstein, E.C., and H. Sievering, Interaction Mechanisms--Within the Atmosphere, in {\it Manual of Remote Sensing}, edited by R.G. Reeves, A. Anson, D. Landen, pp.181-233, American Society of Photogrammetry, Falls Church, VA, 1975.

Gloersen, P., W. J. Campbell, D. J. Cavalieri, J. C. Comiso, C. L. Parkinson, H. J. Zwally, "Arctic and Antarctic Sea Ice, 1978-1987L Satellite Passive Microwave Observations and Analysis," *NASA Spec. Publ.,* Vol. 511, 290 pp, 1992.

Gloersen, P. and D.J. Cavalieri, Reduction of weather effects in the calculation of sea ice concentration from microwave radiances, J. Geophys. Res., 91, 3913-3919, 1986.

Kelly, R.E., A.T.C. Chang, L. Tsang, and J.L. Foster, A prototype AMSR-E global snow area and snow depth algorithm, IEEE Trans. Geoscience Rem. Sens., 41, 230-242, 2003.

Kummerow, C.,On the accuracy of the Eddington approximation for radiative transfer in the microwave frequencies, J. Geophys. Res., 98, 2757-2765, 1993.

Lubin, D., C. Garrity, R.O. Ramseier, and R.H. Whritner, Total sea ice concentration retrieval from the SSM/I 85.5 GHz channels during the Arctic summer, Rem. Sens. Environ., 62, 63-76, 1997.

Markus, T. and D. J. Cavalieri, Snow depth distribution over sea ice in the Southern Ocean from satellite passive microwave data, Antarctic Sea Ice: Physical Processes, Interactions and Variability, Antarctic Research Series, Volume 74, pp 19-39, American Geophysical Union, Washington, DC, 1998.

Markus, T. and D.J. Cavalieri, An enhancement of the NASA Team sea ice algorithm, IEEE Trans. Geoscience Remote Sensing, 38, 1387-1398, 2000.

Markus, T. and S.T. Dokken, Evaluation of Arctic late summer passive microwave sea ice retrievals, IEEE Trans. Geoscience Remote Sensing, 40(2), 348-356, 2002 .

Matzler, C., R.O. Ramseier, and E. Svendsen, Polarization effects in sea-ice signatures, IEEE J. Oceanic Eng., OE-9, 333-338, 1984.